# Multivariate Likelihood Function Measurement of Single-Top-Quark Production with 3.2 fb$^{-1}$ of Data

The CDF Collaboration
*URL http://www-cdf.fnal.gov*
(Dated: February 19, 2009)

We report results from the multivariate likelihood function measurement of single-top production with CDF II data corresponding to 3.2 fb$^{-1}$ of Tevatron data collected at $\sqrt{s} = 1.96$ TeV. Our expected median $p$-value corresponds to a significance of $4.0\sigma$, while the measured $p$-value corresponds to a $2.4\sigma$ excess over the Standard Model background (assuming $M_{top}$=175 GeV). The best-fit value for the combined $s+t$-channel production of single-top quarks assuming the Standard Model ratio of their production cross sections is $\sigma_s + \sigma_t = 1.6^{+0.8}_{-0.7}$ pb.

*Preliminary Results for Winter 2009 Conferences*

# I. INTRODUCTION

According to the Standard Model, in $p\bar{p}$ collisions at the Tevatron top quarks can be created in pairs via the strong force, or singly via the electroweak interaction. The latter production mode is referred to as "single-top-quark" production and takes place mainly through the $s-$ or $t-$ channel exchange of a $W$ boson (Figure 1). The D0 collaboration has published evidence for single-top-quark production with approx. 1 fb$^{-1}$ of data [13, 14], and the CDF collaboration has published evidence for single-top-quark production in 2.2 fb$^{-1}$ of data [15].
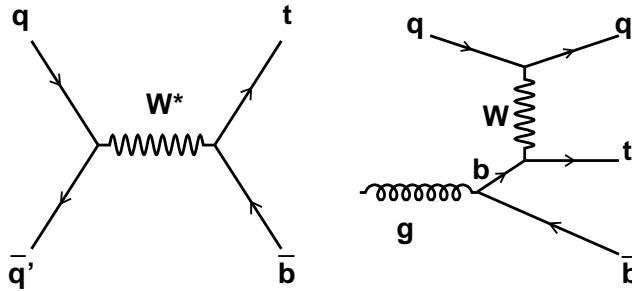


FIG. 1: Representative Feynman diagrams for single-top-quark production at the Tevatron: s-channel $W^*$ (left) and t-channel $W$-gluon fusion (right).

Studying single-top production at hadron colliders is important for a number of reasons. First, it provides a direct window into measuring the CKM matrix element $|V_{tb}|^2$, which is closely tied to the number of quark generations. Second, measuring the spin polarization of single-top quarks can be used to test the $V - A$ structure of the top weak charged current interaction. Third, single-top events are a background to several searches for SM or non-SM signals, for example Higgs boson searches. Fourth and last, the presence of various new SM and non-SM phenomena may be inferred by observing deviations from the predicted rate of the single-top signal.

The theoretical single-top production cross section is $2.864^{+0.40}_{-0.33}$ pb, assuming a top quark mass of 175 GeV/$c^2$ [3]. Despite this small rate, the main obstacle in detecting single top quarks is the large associated background. After all selection requirements are imposed, the signal to background ratio is close to 1/15, and the systematic uncertainties on the background are on the order of 20%. This challenging, background-dominated dataset is the main motivation for using multivariate techniques. The following sections present the event selection, the signal and background estimations, an extended $b$-tagger and a kinematic solver used to improve signal identification, the statistical techniques, the expected and observed single-top cross section results, and a brief summary of these results.

## II. SELECTION REQUIREMENTS

Our selection exploits the kinematic features of the signal final state, which contains a top quark, a bottom quark, and possibly additional light quark jets. To reduce multijet backgrounds, the $W$ originating from the top quark is required to have decayed leptonically. We therefore require the presence of a high-energy electron or muon ($E_T(e) > 20$ GeV, or $P_T(\mu) > 20$ GeV/$c$) inside the pseudorapdity range $|\eta_\ell| < 1.6$. We also require large missing energy from the undetected neutrino $\not{E}_T > 25$ GeV (using jets corrected to the hadron level). We reject dilepton events from $t\bar{t}$ and $Z$ decays, by requiring the dilepton mass to be outside the range: 76 GeV/$c^2 < M_{\ell\ell} < 106$ GeV/$c^2$. The backgrounds surviving these selections can be classified as "non-top" and $t\bar{t}$. The non-top backgrounds are: $Wb\bar{b}$, $Wc\bar{c}$, $Wc$, mistags (light quarks misidentified as heavy flavor jets), non-$W$ (events where a jet is erroneously identified as a lepton), and diboson $WW$, $WZ$, and $ZZ$. We remove a large fraction of the non-top and $t\bar{t}$ backgrounds by demanding exactly two "tight" jets with $E_T > 20$ GeV (corrected to hadron level) and $|\eta| < 2.8$ be present in the event. At least one of the two tight jets should be tagged as a $b$-quark jet by using displaced vertex information from the silicon vertex detector (SVX). The non-$W$ content of the selected dataset is further reduced by imposing a set of requirements on $i$) transverse mass of the reconstructed $W$ boson, $ii$) the $\not{E}_T$ significance (electron events only), and $iii$) the angle between the $\not{E}_T$ vector and the transverse momentum vector of the leading jets (electron events only).

TABLE I: Background and signal estimates for the 3.2 fb$^{-1}$ of data used in this analysis, along with the observed total (last row). The systematic uncertainties on these predictions, as used in the interpretation of the results, are given in Tables II,III and IV.

| Process | 2-jet Prediction | 3-jet Prediction |
|---|---|---|
| $t$-chan | $74.3 \pm 11.0$ | $21.6 \pm 3.2$ |
| $s$-chan | $48.5 \pm 7.0$ | $15.5 \pm 2.2$ |
| $t\bar{t}(\ell + \text{jets})$ | $108.6 \pm 15.8$ | $327.2 \pm 47.3$ |
| $t\bar{t}$ dilepton | $55.9 \pm 8.1$ | $45.9 \pm 6.7$ |
| $Wb\bar{b}$ | $604.6 \pm 182.3$ | $173.0 \pm 52.3$ |
| $Wc(\bar{c})$ | $269.9 \pm 83.2$ | $82.7 \pm 25.5$ |
| $Wc$ | $233.6 \pm 72.1$ | $45.4 \pm 14.0$ |
| $W$+LF | $454.4 \pm 63.6$ | $130.2 \pm 18.6$ |
| $Z$+jets | $27.9 \pm 4.3$ | $10.8 \pm 1.6$ |
| $WW$ | $52.3 \pm 5.9$ | $17.4 \pm 2.0$ |
| $WZ$ | $25.3 \pm 2.1$ | $7.0 \pm 0.6$ |
| $ZZ$ | $0.7 \pm 0.1$ | $0.3 \pm 0.0$ |
| non-$W$ | $82.2 \pm 32.9$ | $33.2 \pm 13.3$ |
| **Total** | $\mathbf{2038.2 \pm 346.2}$ | $\mathbf{910.2 \pm 108.3}$ |
| **Observed** | **2008** | **878** |

## III. SIGNAL AND BACKGROUND ESTIMATIONS

We require rate and kinematic shape predictions for each background source separately with minimal systematic uncertainty in order to test for single top quark production. For some background sources, we are able to use the observed data to constrain their rates and test their shapes, using carefully constructed control samples. Other backgrounds must be estimated with Monte Carlo predictions scaled to theoretical calculations. The $t\bar{t}$, diboson ($WW$, $WZ$ and $ZZ$) contributions, and $Z \to \ell\ell$ are estimated from theoretical predictions. The same can be said about signal estimations.

The background processes for which we can use CDF data to constrain rates and shapes are: $W$+heavy flavor ($Wb\bar{b}$, $Wc\bar{c}$, $Wc$), mistags, and non-$W$ events. Their contributions are obtained using a similar method with that employed in Ref [4], with a few differences. One difference is the larger $\eta$ range for the jet definition ($|\eta| < 2.8$) used in this search. The other difference is that a scale factor for the heavy flavor fraction is used, calculated using taged $W$+1 jet data.

The expected and observed event yields corresponding to the 3.2 fb$^{-1}$ dataset are given in Table I, for both Monte-Carlo based and data based-background estimates.

## IV. SPECIAL EVENT VARIABLES

### A. ANN extended $B$-tagger

An artificial neural network called the KIT flavor separator [5] was developed to increase the $b$-quark purity of the sample selected by the standard $b-$tagging algorithm. The latter is based on measuring displaced (secondary) vertices, and in addition to $b$-jets it also selects a significant fraction of $c-$ and light flavor jets (as much as 50%). The KIT flavor separator is applied to jets selected by the standard $b$-tagger, and exploits mainly the long lifetime (1.6 ps) of $b$-hadrons. Other features used by the neural network are the high $b$-quark mass, the high decay multiplicity, and the decay into leptons. For illustration, Fig. 2 shows good shape agreement between the KIT flavor separator output distributions for the $W + 2$ jet data and a sum of the individual background components normalized to the predicted background rates.

### B. Kinematic Solver

We can use the measured momenta of the final state particles to reconstruct the $W$ boson and the top quark, and constrain the reconstructed masses $M_{\ell\nu}$ and $M_{\ell\nu b}$ to 80.4 GeV and 175 GeV, respectively. The constraint of
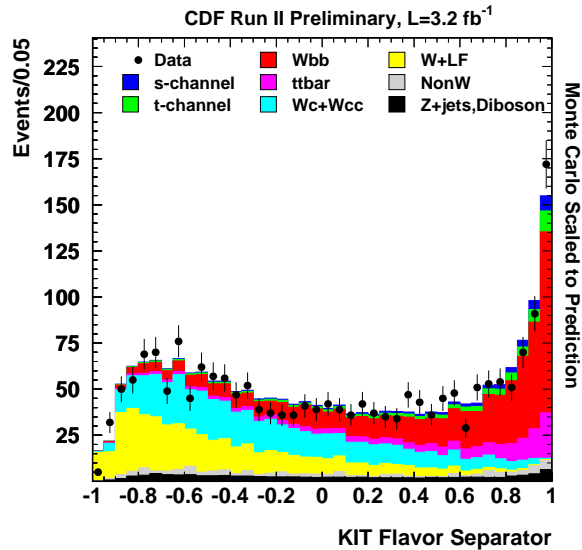
FIG. 2: The KIT flavor separator output distributions for the CDF $W+2$ jets events (points) compared to the Monte Carlo expectations.

the event kinematics to these known masses improves the reconstruction of signal events, worsens the reconstruction of background events, and aids in the separation of the single-top signal from the background. The widths of the top quark and $W$ boson mass distributions at the parton level are of the order of 2 GeV. At reconstructed level the measurement uncertainties are much larger, of the order of 20-40 GeV for $M_{\ell\nu b}$, if one were to use the reconstructed values in the $t$ and $s$ channels, respectively.

The kinematic constraints' use is twofold. First, the $\chi^2$, which is constructed out of the difference between the *measured* jet energies, angles and $\not{E}_T$ and those required by the kinematic constraints, can be used instead of the reconstructed $M_{\ell\nu b}$ as a variable which helps separate signals from backgrounds. The second use of the kinematic constraints is to ensure that the input to the matrix element calculation has four-vectors which correspond to on-shell $W$ bosons and top quarks.

An inventory of the constraints used is as follows:

- The lepton momentum vector is constrained to its measured value.

- The $p_T$ of the top quark is constrained to its measured value.

- The direction and mass of the $b$ jet from top decay are constrained to their measured values.

- $M_{\ell\nu}$ is constrained to 80.4 GeV, resulting in a second-degree equation with two neutrino $p_z$ solutions.

- $M_{\ell\nu b}$ is constrained to 175 GeV.

These constraints are sufficient to solve for the energy of the $b$ jet from top decay, with no regard to its measured value. The ambiguity choices – two possible assignments of the $b$-jet from top decay, and two neutrino $p_z$ solutions (usually), means that the kinematic interpretation must be done four times.

The output from the kinematic solver is a set of neutrino and $b$-jet four-vector solutions, which are used to reconstruct kinematic variables. Also provided is the $\chi^2$ output mentioned above, which indicates how far from the measured values of the $b$-jet energy and the $\not{E}_T$ the solver found its solutions. If the wrong choice of $b$-jet from top is made, then the $\chi^2$ is typically worse than if the correct choice is made, and thus the $\chi^2$ variable can be used to select the $b$ jet in events in which the choice is ambiguous. The $\chi^2$ definition is

$$\chi^2 = \frac{(E_b^{\text{solved}} - E_b^{\text{meas}})^2}{\sigma_b^2} + \frac{(M_{\ell\nu b} - 175 \text{ GeV})^2}{\sigma_{m_t}^2} + \frac{(\Delta \not{E}_T)^2}{\sigma_{\not{E}_T}^2}, \tag{1}$$

where $\sigma_b$ is taken to be 9 GeV, $\sigma_{m_t}$ is taken to be 1 GeV, and $\sigma_{E\!\!\!/_T}$ is taken to be 11 GeV.

## V. LIKELIHOOD FUNCTION TECHNIQUE

No single variable encodes all conceivable signal-background separation, and so a likelihood function [6] is proposed to combine several variables together into a discriminant which can be used to compute limits or to discover a signal.

The likelihood function $\mathcal{L}$ is constructed by first forming histograms of each variable ($n_i$ bins per variable), separately for the signal distributions and for several background distributions, denoted $f_{ijk}$ for bin $j$ of variable $i$ for the event class $k$. For the signal, $k = 1$, and in this note, four background classes are considered: $Wb\bar{b}$, $t\bar{t}$, $Wc\bar{c}/Wc$, and mistags, which are event classes 2, 3, 4 and 5. These histograms are normalized such that $\sum_{j=1}^{n_i} f_{ijk} = 1$ for all $i$ and all $k$. The likelihood function for an event is computed by evaluating in which bin $j_i$ in which the event falls in the distribution of variable $i$, and computing

$$p_{ik} = \frac{f_{ij_i k}}{\sum_{m=1}^{5} f_{ij_i m}}, \qquad (2)$$

which is used to compute

$$\mathcal{L}_k(\{x_i\}) = \frac{\prod_{i=1}^{n_{var}} p_{ik}}{\sum_{m=1}^{5} \prod_{i=1}^{n_{var}} p_{ik}}. \qquad (3)$$

The signal likelihood function is the one which corresponds to the signal class of events, $\mathcal{L}_1$.

Two likelihood functions are computed $- \mathcal{L}_{2j}$ and $\mathcal{L}_{3j}$, using the $t$-channel single-top signal in the signal reference histograms in the two-jet sample and three-jet sample, respectively. Plots of all input variables can be found on the Likelihood Function search public page [16].

### A. Likelihood Function, Two-Jet Sample

The 2-jet bin likelihood function, $\mathcal{L}_{2j}$, uses seven variables, and assumes the $b$-tagged jet comes from top decay. For doubly-tagged events, we set $\mathcal{L}_{2j} = 0$ because the fraction of $t$-channel signal events with two $b$-tags is much lower (of order 3%) while that of two of the main backgrounds, $Wb\bar{b}$ and $t\bar{t}$ backgrounds is closer to 20%. The 2-jet bin $t$-channel likelihood function uses the following seven variables:

 – $H_T$, the scalar sum of the transverse energies of the two tight jets, the lepton, and the missing transverse energy.

 – $Q \times \eta$, the charge of the lepton times the pseudorapidity of the tight jet which is not b-tagged.

 – $\chi_t^2$, output from the kinematic solver for the $t$-channel combination described above.

 – $\cos\theta_{t-\mathrm{chan}}$, the cosine of the angle between the lepton and the untagged tight jet in the top decay frame.

 – $M_{jj}$, the invariant mass of the two tight jets.

 – $\log(\mathrm{ME}_{t-\mathrm{chan}})$, the logarithm of the MADGRAPH matrix element computed using the constrained four-vectors of the $b$, the $\ell$ and the $\nu$.

 – ANN b-tag output.

### B. Likelihood Function, Three-Jet Sample

The 3-jet bin $t$-channel likelihood function, $\mathcal{L}_{3j}$, uses ten input variables. The algorithm used to select the $b$ from top decay is as follows. If there is exactly one $b$-tagged jet in the event, it is used as the $b$ from top decay. In events in which there are two or more tagged jets, only the leading two $b$-tagged jets are considered. The jet with the highest combination of $-\log\chi^2 + 0.005P_t$ is chosen, where $\chi^2$ is the smaller of the two kinematic solver $\chi^2$ outputs, one for each $p_z$ solution of the neutrino, for combinations using that jet as the $b$ from top decay. This algorithm assigns the correct jet to be the $b$ from top decay approximately 75% of the time. The 3-jet bin $t$-channel likelihood function uses the following ten variables:

- $M_{\ell\nu b}$

- ANN $b$-tag output

- The number of $b$-tagged jets

- $q \times \eta$

- The smallest $\Delta R$ of any two jets

- $M_{jj}$ of the two jets not chosen to be the $b$ from top decay

- $\cos\theta_{t-\mathrm{chan}}$

- $p_T$ of the lowest-$E_T$ jet

- $\eta$ of the reconstructed $W$ boson

- $p_T$ of the jet chosen to be the $b$ from top decay

## VI.   SYSTEMATIC UNCERTAINTIES

Systematic variations in the rates and shapes of the likelihood distributions are considered for the signals and backgrounds in the sample. Systematic uncertainties contributing to the shape uncertainties are the jet energy scale (JES), initial state radiation (ISR) and final state radiation (FSR) variations, variations in the NN b-tag output distributions, variations in the flavor composition of the non-$W$ sample, and variation in the $Q^2$ scale in ALPGEN. Shape uncertainties are also assessed for the mismodeling of the $\Delta R_{jj}$ and $\eta_{j2}$ distributions, seen in the taggable-but-not-tagged samples. In the 3-jet bin, the $\Delta R_{jj}$ reweighted was not found to be needed. These same uncertainties contribute to the rate uncertainties, and additional contributions come from the uncertainty in the integrated luminosity, the parton distribution function used, the b-tag scale factor, the $t\bar{t}$ cross section prediction, and uncertainties propagated from the data-based background estimates. Tables II, III, IV V enumerate the relative rate errors on the backgrounds used in the limit calculations.

TABLE II: Fractional systematic rate uncertainties for the two-jet, one b-tag sample, in percent

| Source | $t$-channel | $s$-channel | single-top | $t\bar{t}$ |
|---|---|---|---|---|
| ISR less/more | 2.8/-0.2 | 0.3/6.7 | 1.9/2.1 | -2.6/-7.1 |
| FSR less/more | 4.2/-1.3 | 5.9/0.4 | 4.8/-0.7 | -5.1/-2.6 |
| PDF | 3.1/-3.5 | 1.7/-1.4 | 2.7/-2.8 | 1.9/-2.3 |
| MC | 2.0/-2.0 | 1.0/-1.0 | 1.7/-1.7 | -2.7/2.7 |
| $\epsilon_{evt}$ | 4.2/-4.2 | 2.3/-2.3 | 3.6/-3.6 | 2.9/-2.9 |
| Luminosity | 6.0/-6.0 | 6.0/-6.0 | 6.0/-6.0 | 6.0/-6.0 |
| Cross section | 12.6/-12.6 | 12.4/-12.4 | 12.6/-12.6 | 12.4/-12.4 |
| $M_{\mathrm{top}}$ 170/180 | 1.3/-0.8 | 2.4/-1.7 | 1.7/-1.1 | -3.1/1.4 |
| | Diboson | Z+jets | | |
| $\epsilon_{evt}$ | 7.6/-7.6 | 8.3/-8.3 | | |
| Luminosity | 6.0/-6.0 | 6.0/-6.0 | | |
| Cross Section | 1.9/-1.9 | 10.8/-10.8 | | |

## VII.   RESULTS

We use the likelihood functions described above to search for single-top quark production. The degree to which we have evidence for single-top production is denoted by a $p$-value, which is the probability of observing data at least as signal-like as what we observed. The data are also used to measure the single-top production cross section, using a Bayesian marginalization technique.

A frequentist approach (except in the handling of the systematic uncertainties) is used to determine the $p$-value for single-top production. For $p$-value calculation the 2-jet and 3-jet distributions, $\mathcal{L}_{2j}$ and $\mathcal{L}_{3j}$ were used. The data are compared with two hypotheses. The null hypothesis, $H_0$, assumes Standard Model processes except single-top

TABLE III: Fractional systematic rate uncertainties for the three-jet, one b-tag sample, in percent

| Source | $t$-channel | $s$-channel | single-top | $t\bar{t}$ |
|---|---|---|---|---|
| ISR less/more | -6.8/-0.0 | 2.4/-12.6 | -3.3/-4.8 | -0.6/-4.6 |
| FSR less/more | -1.5/-3.1 | -6.0/-4.8 | -3.3/-3.8 | -3.4/-2.2 |
| PDF | 3.2/-3.7 | 1.5/-1.7 | 2.7/-3.1 | 1.9/-2.3 |
| MC | 1.9/-1.9 | 1.5/-1.5 | 1.7/-1.7 | -1.7/1.7 |
| $\epsilon_{evt}$ | 3.5/-3.5 | 2.3/-2.3 | 3.0/-3.0 | 2.3/-2.3 |
| Luminosity | 6.0/-6.0 | 6.0/-6.0 | 6.0/-6.0 | 6.0/-6.0 |
| Cross section | 12.6/-12.6 | 12.4/-12.4 | 12.6/-12.6 | 12.4/-12.4 |
| $M_{\text{top}}$ 170/180 | 1.5/-2.8 | 6.0/-2.7 | 3.2/-2.7 | -0.7/0.8 |
| | Diboson | Z+jets | | |
| $\epsilon_{evt}$ | 7.8/-7.8 | 7.8/-7.8 | | |
| Luminosity | 6.0/-6.0 | 6.0/-6.0 | | |
| Cross Section | 1.9/-1.9 | 10.8/-10.8 | | |

TABLE IV: Fractional Systematic rate uncertainties for 3-jet 2 tag bin, in percent

| Source | $t$-channel | $s$-channel | single-top | $t\bar{t}$ |
|---|---|---|---|---|
| ISR less/more | 7.8/3.2 | 4.3/-11.2 | 5.8/-4.9 | -0.5/-6.6 |
| FSR less/more | 15.0/1.3 | -7.4/-5.0 | 2.4/-2.2 | -3.4/-2.7 |
| PDF | 3.7/-4.1 | 1.8/-1.5 | 3.1/-3.3 | 1.7/-1.7 |
| MC | 1.9/-1.9 | 1.5/-1.5 | 1.7/-1.7 | 2.0/-2.0 |
| $\epsilon_{evt}$ | 9.1/-9.1 | 8.8/-8.8 | 8.9/-8.9 | 9.1/-9.1 |
| Luminosity | 6.0/-6.0 | 6.0/-6.0 | 6.0/-6.0 | 6.0/-6.0 |
| Cross section | 12.6/-12.6 | 12.4/-12.4 | 12.5/-12.5 | 12.4/-12.4 |
| $M_{\text{top}}$ 170/180 | 4.2/3.0 | 1.6/-6.8 | 2.7/-2.5 | -0.6/-1.0 |
| $\epsilon_{evt}$ | 10.8/-10.8 | 11.1/-11.1 | | |
| Luminosity | 6.0/-6.0 | 6.0/-6.0 | | |
| Cross Section | 1.9/-1.9 | 10.8/-10.8 | | |

TABLE V: Jet Energy Scale uncertainties, in percent

| process | 2jet 1 tag | 3jet 1 tag | 3jet 2 tag |
|---|---|---|---|
| $t$-channel | -1.1/0.6% | -10.4/10.6% | -5.7/4.3% |
| $s$-channel | -0.1-0.6% | -8.3/9.4% | -7.2/7.4% |
| $t\bar{t}$ | 9.8/-9.4% | 4.6/-5.1% | -5.4/5.2% |
| $Wc\bar{c}$ | 7.0/-6.9% | 8.4/-7.7% | 11.0/-12.1% |
| $Wb\bar{b}$ | 7.0/-6.9% | 8.4/-7.7% | 11.0/-12.1% |
| Z+jets | -5.3/5.4% | -10.8/14.0% | -5.0/5.0% |
| diboson | -2.7/1.7% | -12.4/11.9% | -11.0/11.0% |

quark production, while the test hypothesis, $H_1$, assumes all Standard Model processes including single-top quark production, with both $s$-channel and $t$-channel processes at their Standard Model rates. The likelihood ratio is defined as:

$$-2\ln Q = -2\ln \frac{p(\text{data}|H_1,\hat{\theta})}{p(\text{data}|H_0,\hat{\hat{\theta}})}, \qquad (4)$$

where $\theta$ are the nuisance parameters describing the uncertain values of the quantities studied for systematic error, $\hat{\theta}$ are the best-fit values of $\theta$ under $H_1$, and $\hat{\hat{\theta}}$ are the best-fit values of the nuisance parameters under $H_0$. In this case, the 2 -jet and 3-jet results are jointly fit. Two sets of pseudoexperiments are performed, one assuming $H_1$ and the other assuming $H_0$. On each pseudoexperiment, the values of the nuisance parameters are chosen randomly based on the systematic errors. The distributions of the values of $-2\ln Q$ are shown in Figure 4 for both hypotheses, and for the data.

The $p$-value is the probability that $-2\ln Q < -2\ln Q_{\text{obs}}$, assuming the null hypothesis $H_0$. The $p$-value was found to be $9.07 \times 10^{-3}$, which corresponds to a $2.4\sigma$ excess. The sensitivity of the analysis is computed as the median expected $p$-value assuming a signal is truly present. The median $-2\ln Q$ is extracted from the $H_1$ distribution, and the integral of the $H_0$ distribution of $-2\ln Q$ to the left of this median value is the median expected $p$-value. The value thus obtained is $2.58 \times 10^{-5}$, corresponding to $4.0\sigma$.
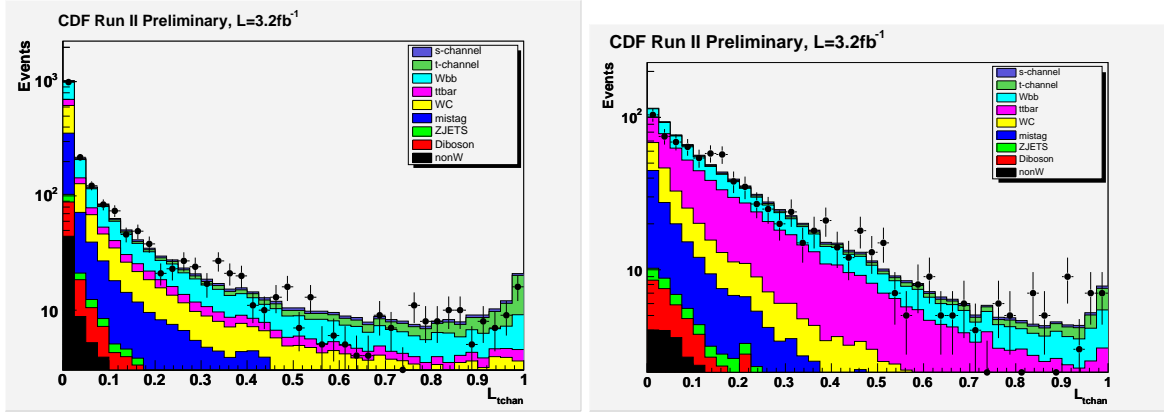
FIG. 3: The distributions of the $t$-channel 2-jet (left) and 3-jet (right) likelihood functions for CDF data compared to the Monte Carlo predictions normalized to the expected SM contributions for 3.2 fb$^{-1}$ of integrated luminosity.
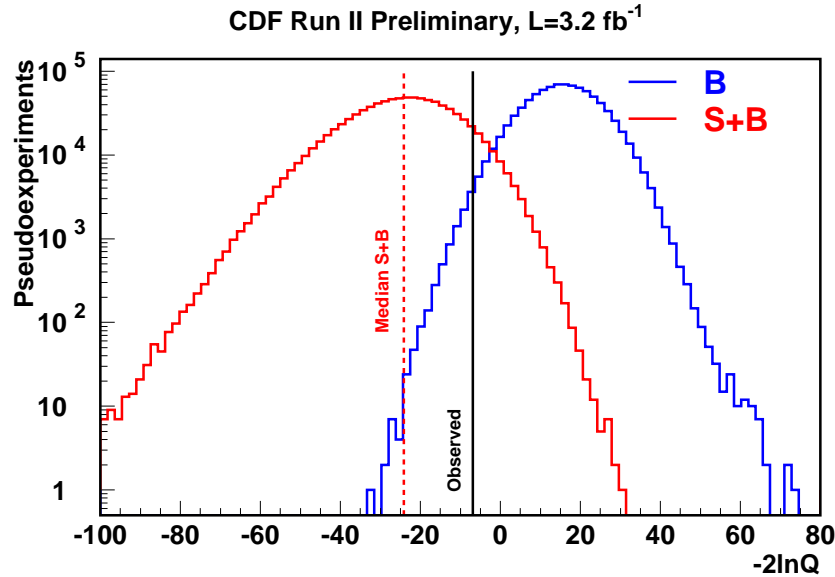


FIG. 4: Distributions of $-2\ln Q$ for the test hypothesis $H_1$, which assumes Standard Model backgrounds plus Standard-Model single-top production (red histogram), and for the null hypothesis, $H_0$, which assumes single-top production is absent (blue histogram). The observed value of $-2\ln Q$ is indicated with a solid, vertical line. The plot is shown on a logarithmic scale. The $p$-value is the fraction of the integral of the $H_0$ curve to the left of the data.

In order to measure the single-top production cross section, a Bayesian marginalization technique is applied to the $t$-channel likelihood output histograms in both the 2-jet and 3-jet samples. The Standard Model ratio between $\sigma_s$ and $\sigma_t$ and a flat prior in $\sigma_s + \sigma_t$ is assumed. The nuisance parameters are integrated out as described in [11],[7]. The distribution of the posterior is shown in Figure 5. The maximum of the posterior is taken to be the best-fit value, and the 68% confidence interval is taken to be the shortest interval containing 68% of the integral of the posterior distribution. The resulting cross section measurment is $\sigma_s + \sigma_t = 1.6^{+0.8}_{-0.7}$ pb.

Using the cross section measurement, we additionally measure $|V_{tb}| = 0.75^{+0.17}_{-0.19} \pm (0.07)(\text{theory})$, and set a limit of
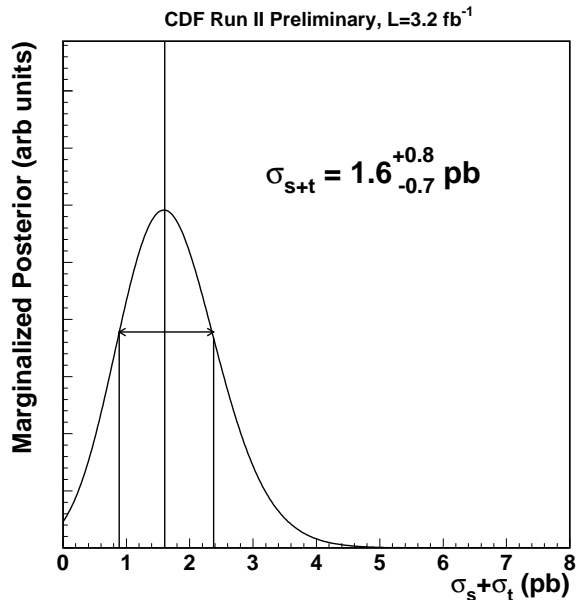
FIG. 5: Fit for $\sigma_s + \sigma_t$. A uniform prior in $\sigma_s + \sigma_t$ is assumed, and the SM ratio of $\sigma_s/\sigma_t$ is also assumed. The Bayesian posterior, marginalized over nuisance parameters, is shown. The maximum value is the central value of the cross-section fit, and the smallest interval enclosing 68% of the integral of the posterior is the quoted interval. The measured result is $\sigma_s + \sigma_t = 1.6^{+0.8}_{-0.7}$ pb.

$|V_{tb}| > 0.41$ at 95% credibility level.

## VIII.   CONCLUSION

We present an analysis of the 3.2 fb$^{-1}$ dataset in search of single-top-quark events, using a multivariate likelihood function technique, with two likelihood functions designed to isolate $t$-channel signal events from the backgrounds, separately in the two-jet and three-jet samples. We find an observed $p$-value of $9.07 \times 10^{-3}$, which corresponds to a $2.4\sigma$ excess over the Standard Model backgrounds. The median expected $p$-value assuming single-top production occurs at the Standard Model rate, is $2.58 \times 10^{-5}$, corresponding to $4.0\sigma$.

We measure the single-top production cross section, assuming that the branching ratio $B(t \to Wb) \approx 100\%$, and that $M_t = 175$ GeV. Assuming further that the ratio between the $s$-channel and the $t$-channel cross sections are as predicted by the Standard Model, the single-top cross section is measured to be $\sigma_s + \sigma_t = 1.6^{+0.8}_{-0.7}$ pb. The Standard Model prediction for $\sigma_s + \sigma_t$ is $2.864^{+0.40}_{-0.33}$ pb [3] (The theory errors on $\sigma_s$ and $\sigma_t$ have been added linearly here, assuming they are 100% correlated).

## Acknowledgments

[1] D. Acosta *et al.* (CDF Collaboration), Phys. Rev. D **65**, 091102 (2002); D. Acosta *et al.* (CDF Collaboration), Phys. Rev. D **69**, 052003 (2004); D. Acosta *et al.* (CDF Collaboration), Phys. Rev. D **71**, 012005 (2005).

[2] B. Abbott *et al.* (DØ Collaboration), Phys. Rev. D **63**, 031101 (2001); V. M. Abazov *et al.* (DØ Collaboration), Phys. Lett. B **517**, 282 (2001); V. M. Abazov *et al.* (DØ Collaboration), Phys. Lett. B **622**, 265 (2005).

[3] B. W. Harris *et al.*, Phys. Rev. D **66**, 054024 (2002); Z. Sullivan, Phys. Rev. D **70**, 114012 (2004).
N. Kidonakis, Phys. Rev. D **74**, 114012 (2006) [arXiv:hep-ph/0609287].

[4] The CDF Collaboration, "Measurement of the Top Pair Production Cross Section in the Lepton+Jets Decay Channel" CDF Note 8795, 2007 (*public*)

[5] T. Chwalek *et al.*, "Update of the Neural Network b Tagger for Single-Top Analyses", CDF note 8903, 2007 (*internal*).

[6] R. Barlow, "Statistics: a Guide to the Use of Statistics in the Physical Sciences" John Wiley and Sons, LTD, West Sussex, England (1989).

[7] T. Junk, "Sensitivity, Exclusion and Discovery with Small Signals, Large Backgrounds, and Large Systematics", CDF note 8128 (*internal*). Also see: A. L. Read, J. Phys. G: Nucl. Part. Phys. **28**, 2693 (2002); P. Bock *et al.* (the LEP Collaborations), CERN-EP-98-046 (1998) and CERN-EP-2000-055 (2000).

[8] M. Feindt, e-Print Archive physics/0402093 (2004).

[9] T. Tait and C. P. Yuan, Phys.Rev. **D63** (2001) 014018, available online as arXiv:hep-ph/0007298 (2000).

[10] Luc Demortier, Louis Lyons, Joel Heinrich, Giovanni Punzi, John Conway, Craig Blocker, Tom Junk, CDF Note 8023 (2006) (*internal*).

[11] J. Heinrich, "Bayesian limit software: multi-channel with correlated backgrounds and efficiencies", CDF note no. 7587 (*internal*).

[12] T. Tait and C. P. Yuan, Phys.Rev. **D63** (2001) 014018, available online as arXiv:hep-ph/0007298 (2000).

[13] V. M. Abazov *et al.* [D0 Collaboration], Phys. Rev. Lett. **98**, 181802 (2007) [arXiv:hep-ex/0612052];
also see: http://www-d0.fnal.gov/Run2Physics/top/top_public_web_pages/top_public.html

[14] V. M. Abazov *et al.* [D0 Collaboration], Phys. Rev. D **78**, 012005 (2008) [arXiv:0803.0739 [hep-ex]].

[15] T. Aaltonen *et al.* [CDF Collaboration], Phys. Rev. Lett. **101**, 252001 (2008) [arXiv:0809.2581 [hep-ex]].

also see: http://www-cdf.fnal.gov/physics/new/top/public_singletop.html

[16] See: http://www-cdf.fnal.gov/physics/new/top/2009/singletop/LF_3.2/LF_32.html